Check for updates

View Article Online
View Journal

CrystEngComm

Accepted Manuscript

This article can be cited before page numbers have been issued, to do this please use: G. F. Teixeira, E. Silva Junior, A. Z. Simoes, E. Longo and M. A. Zaghete, *CrystEngComm*, 2017, DOI: 10.1039/C7CE00218A.

This is an Accepted Manuscript, which has been through the Royal Society of Chemistry peer review process and has been accepted for publication.

Accepted Manuscripts are published online shortly after acceptance, before technical editing, formatting and proof reading. Using this free service, authors can make their results available to the community, in citable form, before we publish the edited article. We will replace this Accepted Manuscript with the edited and formatted Advance Article as soon as it is available.

You can find more information about Accepted Manuscripts in the author guidelines.

Please note that technical editing may introduce minor changes to the text and/or graphics, which may alter content. The journal's standard Terms & Conditions and the ethical guidelines, outlined in our author and reviewer resource centre, still apply. In no event shall the Royal Society of Chemistry be held responsible for any errors or omissions in this Accepted Manuscript or any consequences arising from the use of any information it contains.

ROYAL SOCIETY OF CHEMISTRY

rsc.li/crystengcomm

Please do notadjustmargins
View Article Online
DOI: 10.1039/C7CE00218A

JournalName

ARTICLE

Received 00th January 20xx,
Accepted 00th January 20xx
DOI: 10.1039/x0xx00000x
www.rsc.org/

Unveiling the correlation between structural order-disorder character and photoluminescence emissions of $NaNbO_3$

G. F. Teixeira[a], E. Silva Junior[a], A. Z. Simões[b], E. Longo[a], M. A Zaghete[a]

$NaNbO_3$samples were synthesized via the microwave-assisted hydrothermal method under different processing times (ranging from 30-90 minutes) at 180°C using NaOH as mineralizer. XRD and Rietveld refinement data confirmed the obtention of $NaNbO_3$ with orthorhombic (*Pbma*) crystallographic structure devoid of secondary phases. The Raman scattering spectra revealed that the symmetry of $NaNbO_3$ space group has vibrational modes associated with librations and internal vibrational modes of NbO_6 octahedron.The $NaNbO_3$ particles grow as polyhedral shape highly agglomerated way, assuming plate-like manner, however, as time increases the particles become less agglomerated assuming parallelepiped-like shapes. With increase in the processing time, the optical band gap (3.24 eV (30 min); 3.32 eV (60 min) and 3.34 eV (90min)) showed presents a slight difference in the density of intermediary energy levels within the band gap which affects the electronic transitions. The broad band PL emission (350-800 nm) obtained at room temperature, with a PL sub-band at ~ 455 nm (blue component) dominant, displays that the changes in the electronic density are related to the defects of oxygen vacancies (at bulk and surface) due to the strucutural disorder degree at medium-range, *i.e.*, local distortions of the NbO_6 octahedron as result of the changes in the Nb-O bond lengths and O-Nb-O bond angles, increasing the degree of strctural disorder at medium-range, and thereby a decline in the PL intensity as synthesis time increases. This structural disorder at medium-range is able to transform the $NaNbO_3$ ordered strucuture, which is constituted of $[NbO_6]^x$ clusters, into ordered-disordered $NaNbO_3$structure, formed by $[NbO_5.V_O^x]$, $[NbO_5.V_O^{\bullet}]$ and $[NbO_5.V_O^{\bullet\bullet}]$ complex clusters.

Introduction

Technological development provides us with smart materials endowed with interesting characteristics such as piezoelectric and ferroelectric properties. These materials can be used in energy harvesting devices to convert mechanical energy into electrical energy for a long span of time. This conversion of energy can be accomplished using human body movement as mechanical energy source [1,2]. As a result of its strong piezoelectric response, lead zirconate titanate - $Pb(Zr,Ti)O_3$(PZT) based materials are the most widely employed in energy harvesting devices at present [3,4], even though lead has recently been banned from many commercial applications due to warranted concerns regarding its toxicity [5]. With the decreasing of the employ of this element, an intense effort was spented with the intent of developing lead-free materials with high piezoelectric activity and environmentally friendly. Therefore, an intense effort was mounted to develop lead-free and both highly piezoelectric-active and environmentally compatible materials. For the fact that it has a typical perovskite structure, apart from being highly stable and nontoxic, sodium niobate ($NaNbO_3$) has become one of the most attractive candidates for replacing lead-based materials [6a-c]. By virtue of its wide of properties including good crystallinity, high dielectric constant [7, 8], large electromechanical coupling and high polarization [9], sodium niobate ($NaNbO_3$) has largely spurred great scientific and technological interest for applications in nanodevices and photocalysts [10a-e]. $NaNbO_3$ exhibits a complex structural phase transition [11, 12] which can be induced by temperature [13], pressure [14] and particle size [15, 16]. Among the phases presented by $NaNbO_3$ include orthorhombic, tetragonal and cubic structures [17]. However, this polymorphism has, indeed, not yet been fully understood [18], and many studies have been conducted aiming at understanding the relationship between the parameters such as the crystalline structure and functional properties [9, 18-22].

Normally, at room temperature, $NaNbO_3$ belongs to the crystalline orthorhombic system (*a*= 5.506 Å, *b*= 5.566 Å and *c*= 15.52 Å) with the space group *Pbcm,* where one can observe the occupation of two crystallographic sites by sodium [23, 24, 25]. Darkington and Knight studied $NaNbO_3$ with a lower orthorhombic symmetry by neutron powder diffraction data at room temperature [26], however these experimental evidence still raise large discussion [27, 28]. The combination of techniques such as XRD, neutron powder diffraction, NMR spectroscopy [23] in addition to theoretical approaches [29] have been much more useful in elucidating the occurrence of a secondary symmetry phase (polar phase) $P2_1ma$ and its related space groups ($Pnma$, $Pn2_1a$, $Pnm2_1$) in the $NaNbO_3$orthorhombic crystals. From a structural viewpoint, the

[a]Universidade Estadual Paulista- Unesp- Instituto de Química de Araraquara, Rua Professor FraanciscoDegni 55, Bairro Quitandinha, P.O. Box 355, 14800-900, Araraquara, São Paulo, Brazil, Fone: +55 16 3301-9500; Fax: +55 16 3301-2308.
[b]Universidade Estadual Paulista- Unesp - Faculdade de Engenharia de Guaratingueta, Av. DrAriberto Pereira da Cunha 333, Bairro Pedregulho, P.O. Box 355, 12.516-410,Guaratinguetá, São Paulo, Brazil, Phone: +55 12 3123-2765; Fax: +55 12 3123-2800
*corresponding author: mina.guilher@gmail.com
† Footnotes relating to the title and/or authors should appear here.
Electronic Supplementary Information (ESI) available: [details of any supplementary information available should be included here]. See DOI: 10.1039/x0xx00000x

Published on 25 May 2017. Downloaded by University of Lethbridge on 28/05/2017 21:08:29.
CrystEngComm Accepted Manuscript

Please do notadjustmargins

View Article Online
DOI: 10.1039/C7CE00218A

Published on 25 May 2017. Downloaded by University of Lethbridge on 28/05/2017 21:08:29.

occurrence of these structural phase transitions can be explained by the displacement of Nb of the symmetry center on the [NbO_6] octahedral clusters, as well as by the *tilts* caused by the presence of Na in the interstitial sites of the [NbO_6] octahedral clusters bonded through the vertices [11]. $NaNbO_3$ powders can be obtained by different synthesis methods including solid state reaction [30], Pechini's method [6], molten salt synthesis [31], coprecipitation [32] and hydrothermal method [33a-c].

In the hydrothermal method, the particles are crystallized directly in solution causing better control of the size, morphology and aggregation degree of the particles [34]. Several authors have reported obtaining $NaNbO_3$ powders by direct reaction between Nb_2O_5 and NaOH via the hydrothermal method at long processing time, with the presence of a polymorphism [33 (a,c), 35]. In these cases, NaOH can be used as sodium source and a mineralizing agent for the control of pH. The use of templates, such as polyamide (PA), ethylene glycol (EG), ethylenediamine (EN), polyvinyl alcohol (PVA) or pluronic P-123 [35, a,b] becomes essentially necessary when a specific morphology is required.

The heat treatment in the conventional hydrothermal method is performed using heat conductive mechanism from the conventional source, *e.g.* electrical resistance or oil bath [36a,b]. This enables the regions of the solution in contact with the vessel walls to heat more quickly, resulting in a thermal gradient in the reaction medium [37a,b]. This temperature gradient in the reaction medium generates convection currents within the solution tending towards equilibrium in high processing periods [38a,b].

The major drawback of the heat conductive mechanism employed in conventional hydrothermal methods lies in the long span of time required to reach thermal equilibrium. Remarkably, with their advent in the early 70^s, microwave heating devices soon became popular in chemistry, mainly in experiments with regard to the decomposition of organic molecules (alcohols, ketones, ester, etc.) [39 a,b,c]. Clearly, under microwave irradiation, decomposition reactions were processed in few minutes. With the continuous progress of the microwave-assisted chemistry, researchers found yet more advantages of microwave heating compared to conductive heating which included the benefits of attaining uniform and fast heating, increasing the kinds of mechanisms involved in the thermal/kinetic effects, and consequently decreasing the processing time while at the same time ensuring energy saving [40,a,b,c].

In this context, in quest for solving the problems of thermal gradients and slow heating rate in conventional hydrothermal methods, researchers began using microwave radiation in hydrothermal methods which became known as microwave-assisted hydrothermal methods (MAH). The possibility of increasing the boiling point of certain solvents and keep the liquid phase under hydrothermal conditions, coupled with the unique nature of the microwave dielectric heating mechanism, are factors that essentially contribute towards increasing the thermal/kinetics effects of the reaction rate by a factor between 10-1000 [41a,b], making the hydro/solvothermal methods via microwave heating an interesting and advantageous alternative in certain cases. Abu-Sharma et al. [42] reported the quick dissolution of some inorganic mineral acids by an order of magnitude when subjected to microwave radiation under hydrothermal conditions (≤ 200 °C and 10-20 bars).

Previous works of our research group have been devoted towards the synthesis of different $NaNbO_3$ polymorphs [33b, 43]. Paula et al. [33 b] reported obtaining cubic $NaNbO_3$ particles by modulating the precursor concentration and the synthesis times. The authors identified $Na_2Nb_2O_6.H_2O$ intermediate phase with fiber morphology during $NaNbO_3$ crystallization. $Na_2Nb_2O_6.H_2O$ can be used as precursor of $NaNbO_3$ with one-dimensional morphology. In this case, $Na_2Nb_2O_6.H_2O$ is heat-treated to convert the $Na_2Nb_2O_6.H_2O$ crystalline structure into $NaNbO_3$ crystalline structure, maintaining one-dimensional morphology [43, 44].

In this present study, we propose to obtain $NaNbO_3$ in a unique phase by means of a simple and fast synthetic route based on the MAH method. From $NaNbO_3$ structures, we seek that these novel results can arouse enough interest since they contribute towards broadening the fundamental knowledge of $NaNbO_3$-based compounds, bringing to light to relationship between the photoluminescence (PL) emissions and structural order-disorder degree at long-medium-short range. We have a long-term experience when it comes to studying the dependence of PL behavior on structural and electronic order-disorder effects, as well as the structural evolution of perovskite-based materials. The obtained $NaNbO_3$ particles were analyzed using X-ray diffraction (XRD) with Rietveld refinement, Raman scattering spectroscopy, field-emission scanning electron microscopy (FE-SEM), ultraviolet-visible (UV-vis) spectroscopy, and photoluminescence (PL) spectroscopy at room temperature.

Experimental

Materials and methods

The microwave-assisted hydrothermal synthesis of $NaNbO_3$ powders was performed starting with a suspension containing 0.696 g of NaOH (p. a. Quemis) and 8.0 mol.L^{-1} of Nb_2O_5 (Alfa Aesar, 99%) aqueous solution. In this case, the NaOH acts as mineralizing agent and sodium source. The reaction was carried out within a Teflon® vessel model XP-1500 (CEM Corp.), assisted by microwave digestion MARS-5 (CEM Corp.) at 180 °C and an output power of 800 W in different processing times (30, 60 and 90 minutes). The products were thoroughly washed with water by centrifugation and finally dried at room temperature. The $NaNbO_3$ obtained particles were characterized by X-ray powder diffraction (XRD) using a diffractometer model Rigaku-DMax/2500PC (Japan) with Cu-Kα radiation (λ = 1.5406 Å) in the 2θ range of 10° to 120° with 0.02^0 min^{-1}. The Raman scattering spectra were collected by means of a triple monochromator T-64000 HORIBA Jobin-Yvon (USA) coupled to a CCD detector with excitation of 514.4 nm of an argon ion laser, with input power of 8 mW. The morphology of the as-prepared materials was observed through field-emission scanning electron microscopy (FE-SEM) using a microscope model Supra 35-VP (Germany) operated at 5 kV. Ultraviolet–visible absorption spectroscopy (UV-vis) in diffuse reflectance mode was performed through a Varian spectrophotometer model Cary 5G (USA). Photoluminescence (PL) measurements were carried out through a Monospec 27 monochromator of Thermal Jarrel Ash (USA) with a photomultiplier Hamamatsu R446 (Japan). The 350 nm excitation of a krypton ion laser of Coherent Innova (USA) was applied, where nominal output power was kept at 550 mW with maximum power of 40mW on the samples after passing through an optical chopper. All measurements were performed at room temperature.

Results and discussion

X-Ray diffraction and Rietveld refinements analyses

As it has been widely reported in the literature [9, 10, 11, 23 and 24], the presence of several $NaNbO_3$ polymorphs renders the

CrystEngComm Accepted Manuscript

Please do notadjustmargins
View Article Online
DOI: 10.1039/C7CE00218A

Published on 25 May 2017. Downloaded by University of Lethbridge on 28/05/2017 21:08:29.

determination of the $NaNbO_3$ unit cell system as well as the space group quite unwieldy [26, 27]. To circumvent this problem, the Rietveld refinement method [45, 46 (a, b)] was employed aiming at determining, with great accuracy, the structural parameters related to the degree of $NaNbO_3$ structural ordering at long range.

In practical viewpoint, the Rietveld refinement analysis employed the least-squares approach where each cycle generated a diffraction pattern which is monitored until the best fit is obtained between the observed sample diffraction compared to the theorical pattern. A representative model close to the actual structure of the sample is obtained, where parameters related to crystal structure, optical diffraction effects, instrumental factors, background radiation, and other characteristics of the sample are concomitantly refined by adjusting what can be modelled according to the nature of each sample [45, 46, 47, 48,49]. These fitting parameters are expressed by indices called discordance factors, and they play a key role in determining the quality of the adjustment at the end of each cycle. The main indices that constitute the factors include the following: R_{wp} – weighted factor profile, R_{exp} - expected weighted factor profile, R_B - Bragg factor, and χ^2 – reduced Chi-square [46 a, b]. For one to obtain a good refinement, at the end of the process the χ^2 must have reached values close to 1.0, *i.e.*, the R_{wp} must reach an "ideal" value which can be expected for an observed diffraction pattern statistically reliable. In this work, we use the software GSAS (General Strucuture Analysis System) developed by A. C. Larson and R. B. Von Dreele [50] with graphic interface EXPGUI created by B. G. Toby [51] to perform the Rietveld refinement analysis. The optimized parameters included scale factor, background (Chebyshev function), exponential thermal shift, crystal strucuture, size strain (anisotropy with no rules), profile half-width parameters (*u*, *v*, *w*), texture and lattice parameters (*a*, *b*, *c*), preferred orientation and atomic site occupancies (Wyckoff) [50].

Figure 1: XRD patterns from Rietveld refinement method of $NaNbO_3$ heat-treated at 180 °C by the MAH method under different processing times.

The as-prepared $NaNbO_3$ XRD patterns from Rietveld refinement, experimental lattice parameters, and the reliability index are depicted in Fig. 1 and Tab. 1, respectively. The XRD patterns shown the same profile regardless of the processing time (Fig. 1), as such no peak of any other $NaNbO_3$-phase was detected. In other words, the structural order at long range was kept. Thus, the crystalline structure for the as-prepared $NaNbO_3$ materials can be well-indexed to a pure orthorhombic crystal structure of $NaNbO_3$ (space group-*Pbma*) according to the crystallographic information file (CIF n°. 97669) available on the Inorganic Crystal Structure Database (ICSD) [52].

Generally, in the conventional hydrothermal method, the $Na_2Nb_2O_6{\cdot}H_2O$ metastable phase is present during $NaNbO_3$ crystallization [53]. According to Wu et al., $NaNbO_3$ formation is favored by the increase in processing time owing to dissolution rate of Nb_2O_5 in NaOH medium [54]. However, our investigation here showed that no metastable phase is observed with the use of microwave heating under hydrothermal conditions. This occurs largely because the dissolution of Nb_2O_5 under microwave irradiation is faster [55], *i.e.*, the thermal effects under the reaction rates of the precursors (Nb_2O_5 and NaOH) are enhanced by the microwave power, thereby contributing towards preventing the formation of metastable intermediate phases which promote the transformation of $NaNbO_3$ instead of $Na_2Nb_2O_6{\cdot}H_2O$.

As can be seen in Tab. 1, the values related to the reliability factors (R_{wp}, R_{exp}, and χ^2) suggest that a good fit was reached. The values obtained were very close to those reported in the literature [52, 56]. In comparison to the values related to the theoretical approach (CIF n°. 96779), considerable variations were observed from the Rietveld refinement method, in the atomic positions (x, y, z) mainly for Na2, Nb1, O3 and O4 atoms (see Tab.1). Another appreciable variation occurred in the lattice parameters (*a*, *b*, *c*) and unit cell volume. These results indicate the existence of structural distortions on the crystalline lattice as a result of the displacements of the atoms formers (Na) and modifiers of lattice (Nb and O) in the perovskite structure.

Table 1: $NaNbO_3$ lattice parameters and reliability factors from the Rietveld refinement method.

In a typical $NaNbO_3$ structure, the sodium occupies interstitial sites located in the unit cell vertex, forming twelve-coordinated Na sites (Na1 and Na2), while niobium occupies the octahedral site (Nb1). For the orthorhombic structure, the NbO_6 is linked by vertex to each NbO_6 neighbor forming a deflection due to distortions caused by the presence of Na atoms situated on the octahedral sites, which have an ionic radii (1.32 Å) when is 12-fold coordinated by oxygen, a condition seen to be enough for promoting octahedral deflection [11, 8f].

All perovskites (ABO_3) that maintain the A and B sites coordinated with oxygen, display an octahedral *tilting*, as such for the rhombohedral structure, the BO_6 octahedron experiences *tilting* around each axis. On the other hand, for the orthorhombic structures, these distortions occur around the *b* and *c* axes [57]. The degree of octahedral *tilting* (known as tolerance factor (*t*)) will depend upon ionic radii of the A and B cations [58, 59]. In the "ideal" cubic perovskite-type structure, we have $t = 1$. Nonetheless, deviations around these values occur when the structure undergoes intense distortions via [BO_6] *tilting*, causing it to depart from the cubic symmetry [60]. By solely considering the analysis of the tolerance factor, *i.e.*, taking only geometric aspects into account, at room temperature, in general the perovskite structure of the oxides are stable within the range of $0.75 < t < 1.00$. When $t < 1.00$, the perovskite structure is distorted and may present ferroelectric behavior [60, 61]. Thus, the structure is confirmed to transform from cubic toward orthorhombic (cubic→orthorhombic) [62]. In cases whereby $NaNbO_3$ presents sufficient variations in the Nb-O bond lengths and O-Nb-O bond angles, accompanied by displacements of Na within the lattice capable of promoting octahedral *tilting* and the *t*-values ranging from ~1.00 to 0.949.

Thus, taking into account the aforementioned brief considerations regarding the distortions in the perovskite-type structure, and based on the XRD patterns and Rietveld refinement data, it appears reasonable to admit that despite being ordered at long range, the $NaNbO_3$ obtained by the MAH method shows a structural disorder associated with distortions (*tilts*) of the NbO_6 octahedron. Probably, the changes in the Nb-O bond lengths and O-Nb-O bond angles, as well as the displacement of Na within the $NaNbO_3$ lattice, according to results shown in Tab.1, demonstrate that both Na and Nb are displaced within the lattice. In other words, the structure of the as-prepared $NaNbO_3$ exhibited more distorted clusters compared to the theoretical one.

The specificities of each experimental procedure during the material preparation, such as the synthesis method (hydrothermal, sol-gel, coprecipitation, sonochemical, etc.), as well as the experimental variables (temperature, pressure, time processing,

CrystEngComm Accepted Manuscript

Please do notadjustmargins

View Article Online
DOI: 10.1039/C7CE00218A

Published on 25 May 2017. Downloaded by University of Lethbridge on 28/05/2017 21:08:29.

heating rate, solvents, heating source, etc.) can lead to an increase or decrease of the intrinsic defects (oxygen vacancies, bond lengths and bond angles variations, distortions on the lattice, etc.) [63 a-d], besides exerting influence over the particles size distribution control, morphology, and crystallographic orientations [64 a,b].

With the aim of investigating the degree of distortions of the NO_6 octahedron, the unit cells of the as-prepared $NaNbO_3$ were modelled using the visualization for electronic and structural analysis (VESTA) program version 3.1.8 for Windows [65], along with the lattice parameters and atomic positions obtained from the Rietveld refinement data.

Unit cell representations of $NaNbO_3$

To build the model of the $NaNbO_3$ structure (Fig. 2) from the VESTA software, the lattice parameters and atomic positions presented in Tab. 1 were used. Clearly, the relaxation of the lattice as a result of the variations in the unit cell volume, the atomic position shift (*x*, *y*, *z*) of $NaNbO_3$ structures obtained by MAH in comparison to $NaNbO_3$ theoretical structure ($NaNbO_3$ CIF-96779), and lattice parameters (see Tab. 1) are strong evidence that the $NaNbO_3$ structure shows distortions in the lattice, which might change its optical and electrical properties. The full description of the crystalline structure of the as-prepared $NaNbO_3$ obtained from the MAH method can thus be given as pervoskite-type orthorhombic structures with the space group *Pbma*, point group symmetry of $(D_{2h}^{11})_2$ and eight asymmetric units per unit cell (Z = 8) [52, 66].

According to the literature, the differences in the O–Nb–O bond angles and Nb-O bond lengths can lead to distinct levels of structural order-disorder and/or distortions [56]. However, the development of *ab initio* calculations of ^{23}Na NMR parameters [17, 21, 33 (b,c), 56, 67] have demonstrated that variations in the Na-O and Na displacement within the lattice are generally small and tend to fall when Na is coordinated by a larger number of atoms at greater distances, as in the case of a perovskite-type structure [67 a-d]. In this sense, here we decided to investigate only variations in the O–Nb–O bond angles and Nb-O bond lengths in the formation of $NaNbO_3$ crystal structure. Tables S1, S2, S3, and S4 (see supporting information) provide detailed depiction of some parameters (bond lengths, bond angles, polyhedral volumes, distortion index and effective coordination number) related to the NbO_6 octahedron of the as-prepared $NaNbO_3$ and $NaNbO_3$ (CIF ICSD n° 97666). Tab. 2 briefly shows the main parameters associated with the geometry of NbO_6 octahedron, this can be useful in investigating the lattice distortions. As can be observed, the parameters investigated are distinct from the theoretical values (CIF ICSD n°. 9766) as well as between different samples of $NaNbO_3$ obtained in this work.

Fig. 2 Unit cell representations of $NaNbO_3$ obtained by MAH method.

Table 2. Bond lengths (Nb-O), bond angles (O-Nb-O), polyhedral volume, and coordination number of the NbO_6 octahedron of $NaNbO_3$ obtained via the MAH method and the theoretical values reported in the literature (CIG ICSD n°. 9766).

Generally, the changes observed between the theoretical values and the "experimental" ones confirm that the orthorhombic structure of the as-prepared $NaNbO_3$ is more distorted than the theoretical $NaNbO_3$ which can be considered as "ideal" structure (see Tab. 2). In this sense, there were variations in all the parameters observed associated with the geometric aspects of the NbO_6 octahedron, once these species (NbO_6) are responsible for maintaining the structural ordering for being the lattice forming agents [11, 8f]. On the other hand, the increasing of processing time gave rise to structural defects in the form of distortions of the NbO_6 octahedron. In view of that, the as-prepared $NaNbO_3$ processed in different synthesis times tends to present a local structural disorder, probably at medium and/or short range, owing largely to the changes in the bond lengths (Nb-O) and bond angles (O-Nb-O). This behavior exerts an influence on the polyhedral volume, degree of distortion, and differences in the local coordination environment.

Raman scattering analyses

Raman scattering spectroscopy is a powerful technique useful in providing structural information about structural ordering at short range. According to Ross [69], $NaNbO_3$ crystals present internal modes associated with [NbO_6] octahedron and lattice transitions related to the movement of the cations on the lattice [70,71]. An isolated NbO_6 octhedron with O_h point group has six vibrational modes ($A_{1g}(\nu_1)$ + $E_g(\nu_2)$ + $2F_{1u}(\nu_3, \nu_4)$ + $F_{2g}(\nu_5)$+ $F_{2u}(\nu_6)$). The A_{1g}, E_g, and F_{2g} modes are Raman active, whereas F_{1u} mode is infrared active and F_{2u} mode is inactive [33 b]. These vibrational modes can be classified into two pure bond stretching vibrations of symmetry ($A_{1g}(\nu_1)$ and $E_g(\nu_2)$), two interbond angle bending vibrations ($F_{2g}(\nu_5)$ and $F_{2u}(\nu_6)$), and two vibrations ($F_{1u}(\nu_3)$ and $F_{1u}(\nu_4)$) [69]. Although the F_{2u} mode is Raman inactive, and the F_{1u} mode is infrared active only, their appearance can be observed in the Raman spectrum as a consequence of the multiple unit cell interactions which are responsible for the relaxation of the selection rules [33 b]. Normally, in typical $NaNbO_3$ Raman spectra, the bands situated between 50-100 cm^{-1} are related to Na^+ translational movements, while those in the range of 160-950 cm^{-1} are associated with the internal vibrational modes of NbO_6 octahedron. Accordingly, the bands between 100-180 cm^{-1} arise from librations or rotational vibrations of the NbO_6 octahedron [9, 19].

The Raman spectra of $NaNbO_3$ obtained by the MAH method in different processing times as well as the Raman active vibrational modes are displayed in Fig. 3 and listed in Tab. 3, respectively. The profile spectra are the same for all samples, suggesting a structural ordering at short range. The region between 180 to 276 cm^{-1} refers to the triply degenerated $F_{2g}(\nu_5)$ and $F_{2u}(\nu_6)$ vibrational modes, whereas the bands around 429 cm^{-1} are attributed to the antisymmetric bending mode $F_{1u}(\nu_4)$.The most intense band region is constituted of $E_g(\nu_2)$ and $A_{1g}(\nu_1)$ vibrational modes situated at 560 cm^{-1} and 600 cm^{-1}, respectively. While the region around 670 cm^{-1} can be constituted of the $F_{1u}(\nu_3)$ mode [13], this mode is not present in the $NaNbO_3$ spectra of this present work. The band close to 605 cm^{-1} represents the ν_1 mode which corresponds to a totally symmetric stretching of NbO_6. In cases where there is an occurrence of splitting in this band, this occurrence can be attributed to the distortions of the NbO_6 octahedron [71]. As can be noted in Fig. 3, the band at 600 cm^{-1} does not show any splitting as a function of the processing time, this suggests that the NbO_6 structure in the lattice is kept ordered ensuring the structural ordering at short range. The last weak band at 870 cm^{-1} is related to the combination of the vibrational modes ν_1+ν_5, which is an irreducible representation of the F_{2g}.mode associated with the Nb-O stretching vibration [71].

CrystEngComm Accepted Manuscript

Please do notadjustmargins
View Article Online
DOI: 10.1039/C7CE00218A

Published on 25 May 2017. Downloaded by University of Lethbridge on 28/05/2017 21:08:29.

Fig. 3: Raman scattering spectra of $NaNbO_3$ obtained by the MAH method for different processing times (30, 60 and 90 minutes).

Table 3. Raman bands position observed in the Raman scattering spectra of $NaNbO_3$ obtained by the MAH method at different processing times compared to the literature.

Chang et al. [73] reported that the downward shift in the Nb–O stretching bands, namely v_1 and v_2 modes of $NaNbO_3$ orthorhombic structure (P -phase), is attributed to the displacement of 0.13 Å undergone by niobium ions from the geometrical center of the regular octahedron. However, no shift is observed in the Raman spectra of this present investigation. Thus, the processing time fails to provide any meaningful change in the structural ordering at short range. As a result, based on the XRD and Raman scattering results, it is remarkably plausible to say that $NaNbO_3$ structure is ordered at both short and long ranges relative to the processing time. At medium range, however, its structure might display a local disorder which can be attributed to the changes in the NbO_6 octahedron parameters (volume, angle and length bond, etc.) confirmed by Rietveld refinement.

Compared to the literature (see Tab. 3), the Raman vibrational modes presented in this work are displaced. These deviations can be attributed to the fast microwave heating, which the heating mechanism tends to provide peculiar steps of nucleation, growing and crystallization, thereby leading to a specific structural organization. The particular structural organization caused by the hydrothermal microwave method has been reported in a previous work by our research group for several materials [6, 33 a-b, 64 (a,b), 74c, 75(a,b,c)].

FE-SEM: images analyses and growth mechanism

FEG-SEM micrographs of $NaNbO_3$ obtained at different synthesis times are shown in Fig. 4. Interestingly, the $NaNbO_3$ architecture is composed of many particles which exhibit a layered pattern. The particles can self-assemble, forming agglomerates with polyhedral architecture that tend to assume a parallelepiped-like shape in the absence of any specific additives or templates (Fig. 4 a-c). Fig. 4d shows that under 30 minutes of processing, the $NaNbO_3$ polyhedral plate-like particles are highly agglomerated. When the processing time reaches 60 minutes, the particles grow into parallelepiped-like structures with a better morphologic definition and lower agglomeration degree (Fig. 4e). By increasing the processing time to 90 minutes, the particles maintain the same shape, though becoming larger and more agglomerated with a rough surface (Fig. 4f).

Fig. 4: FE-SEM images of $NaNbO_3$ particles obtained by the MAH method for distinct processing times: (a-d) 30 min. (b-e) 60 min and (c-f) 90 min.

The particles growth occurs due to the simultaneous dissolution and recrystallization processes illustrated in Fig. 5. First, under microwave irradiation, one notices the rapid dissolution of Nb_2O_5 in NaOH medium, promoting the growth of plate-like particles. As the processing time is increased, the particles tend to take on parallelepiped-like shape, decreasing the agglomeration rate. The continuous microwave input power promotes the dissolution of $NaNbO_3$ particles according to Ostwald Ripening mechanism [76]. In this case, smaller particles from the plate-like particles in solution are dissolved and subsequently deposited on the surface of larger particles present in the reaction medium aiming at reaching a more thermodynamically stable stage. Finally, at this stage, the re-crystallization process occurs providing the particles with a distinct structural organization. The Ostwald Ripening process is much explored in hydrothermal synthesis [74 a, b, c].

Figure 5: Growth mechanism of $NaNbO_3$ particles obtained by MAH.

Zhu et al. [53] studied the morphological evolution of $NaNbO_3$ obtained by conventional hydrothermal synthesis. According to the authors, NaOH breaks the bonds between Nb-O of NbO_6 octahedral structure linked by the vertices existent in Nb_2O_5, leading to a structural reordering, inducing the obtaining of the metastable phase in fiber-like shape. Given a rise in the synthesis time, the metastable phase undergoes a reordering process so as to form a stable phase of $NaNbO_3$ in cubic shape. The absence of intermediate metastable fiber-like particles in our work is due to the use of high microwave power that promotes the crystallization of $NaNbO_3$ particles in a short synthesis time.

UV-visible spectroscopy

According literature, the electronic transitions allowed for $NaNbO_3$ exhibit an optical absorption spectrum from indirect electronic transitions ($n = 2$) between the top of the valence band and the bottom of the conduction band [56, 77,]. Its electronic structure is formed by a conduction band from Nb 4d orbital and a valence band from O 2p orbital [8 b,c,f]. However, the structural ordering can lead to significant changes in the optical band gap, so that the energy is generally smaller (around 0.2 eV) in the cubic $NaNbO_3$ unlike in the orthorhombic $NaNbO_3$. This difference is attributed to the variant octahedral ligand field [77].

To estimate the optical band gap (E_{gap}), we used the Kubelka-Munk method [78], which is described in detail in the supporting information. Fig. 6 illustrates the UV-vis spectra of the $NaNbO_3$ obtained by the MAH method processed at 180 °C for 30, 60, and 90 minutes.

The optical band gap for $NaNbO_3$ orthorhombic structure were 3.24, 3.32 and 3.34 eV, for processing times of 30, 60 and 90 minutes, respectively (Fig. 6). For the $NaNbO_3$ orthorhombic structure, Zielinska et al. [79] reported obtaining 3.34 eV; Shi et al. [90] obtained around 3.4-3.5 eV; while Li et al.[56] evaluated 3.29-3.45 eV. These differences were attributed to the different defects present in the structure which arises from the different synthesis method employed in each work. Ferri et al. [80] reported that in perovskites of type $SrTiO_3$, the increase in E_{gap} of $SrTiO_3$ was attributed to reduction of intermediary energy levels within the band gap for disordered structures. In this context, the results for the as-prepared $NaNbO_3$ imply that the E_{gap} is related to the order-disorder structural degree as a result of defects. Thereby, while slightly small, but enough able, the increase in the E_{gap} with processing time is a plausible evidence of the decline of defects [77,80], resulting in a better degree of crystallinity for the $NaNbO_3$ particles processed at 60 and 90 minutes. Despite that 30 minutes of processing, the $NaNbO_3$ structure exhibits a high degree of crystallinity confirmed by the structural order at long- and short-range, the processing time span (30 minutes) tends to generate a structural defects density, probably related to local distortions on the NbO_6 octahedron, giving rise to a larger density of intermediary energy levels within band gap, confirmed by the lowest E_{gap}.

CrystEngComm Accepted Manuscript

Please do notadjustmargins

View Article Online
DOI: 10.1039/C7CE00218A

Published on 25 May 2017. Downloaded by University of Lethbridge on 28/05/2017 21:08:29.

Fig. 6: UV-visible spectra of $NaNbO_3$ obtained by microwave hydrothermal method for different processing times: (a) 30 min. (b) 60 min and (c) 90 min.

PL emission

It is well-established the relationship between the structural order-disorder and defects [6, 43, 63, 64 (a,b), 75 (a, b, c]. The defects can modify the electronic band structure of a wide range of materials, thereby affecting properties such as photoluminescence, which is governed by electronic transitions [64 (a,b,c), 75(a, b, c)]. The PL emission bands can be attributed to different types of electronic transitions allowed that occur between energy levels generated within the band gap [83]. In $NaNbO_3$, the PL emission is based on the local structure of NbO_6 octahedron and the variations in the octahedral ligand field [76]. By similar structural analyses, NbO_6 assumes a regular ordering of the octahedron formed by the strong covalent bonding due to the orbital hybridization between Nb d and O 2p [83 (a, b)]

Fig. 7 shows the PL spectra of $NaNbO_3$ synthesized via the MAH method at 180 °C for 30, 60, and 90 minutes at room temperature. As can be clearly observed, all samples present a broad band emission in the range of 350 to 850 nm. The centers of these broad bands are situated around 460 nm and the emission intensities are seen to decrease with increase in processing time.

Fig. 7: Photoluminescence spectra of $NaNbO_3$ powders obtained by MAH method at 180 °C for different processing times: (a) 30 min. (b) 60 min and (c) 90 min.

The broad band PL emission (Fig. 7) is characteristic of a mechanism by which the relaxation processes occur between intermediary levels generated within the band gap. The differences observed in the PL bands profiles (intensity and broadening) are related to the deviations of E_{gap} as increase processing time. The PL emission of most semiconductors and prevoskites-based materials presents a broad band profile owing to multilevel process that occurs from several paths between intermediary energy levels within the band gap [6, 8 c, 33, 63, 64 (a,b), 74 (a-c), 75 (a, b, c)]. To deeply investigate the contribution of each individual component (PL sub-bands), it was necessary to deconvolute the PL spectra. The deconvolution was performed using PeakFit [83] to fitting the PL bands and tuning parameters such as peak positions and their corresponding areas. Through the PeakFit software, the PL broad bands are known to be composed of PL sub-bands with more than one component (Fig. 8). Aiming at better comparison parameters among all samples, the emission center of each sub-band was fixed and the contribution of each component was analyzed varying the occupied percentage area. In 30, 60, and 90 minutes of processing, the PL sub-bands were defined as blue, green, and yellow components, with maximum values around 455, 530 and 610 nm, respectively (see Tab. 4).

Fig. 8: Deconvolution of PL spectra of $NaNbO_3$ powders obtained by microwave hydrothermal method for different processing times: (a) 30 min. (b) 60 min and (c) 90 min.

It can be noted in Fig. 7 that PL profiles exhibit decreasing in the intensity and broadening, *i.e.,* the full width at half maximum (FWHM) tend to increase as increase processing time (see Tab. 4). Similarly, the contributions of blue and green components undergo a decline while the yellow component rises, when the processing time increases, which can be verified by decreasing of FWHM of each PL component (see Tab. 4).

Table 4: PL intensity, FWHM and peaks centers of the broad band profiles and PL components of $NaNbO_3$ obtained by MAH method at different processing time compared with literature.

It is a known fact that for most semiconductors and perovskite-oxides, the presence of defects, such as lattice distortions, generates shallow levels that represent intermediate energy levels responsible by the PL emission in high energy regions (violet/blue region) in general assigned to the structural defects. Conversely, deep levels give rise to PL emissions in low energy regions (green, yellow, and red region) which are generally associated to the surface defects [84 a-e].

All $NaNbO_3$ materials obtained in this work are structurally ordered at long and short range, in agreement with Rietveld refinement and Raman scattering results, respectively. However, the UV-vis results show that changes in the optical bad gap energy reflect the presence of defects, probably at medium range, which tend to decrease with processing time. Similarly, the PL spectra profiles also point to the existence of defects. The area of each PL component is related to the defects density generated along of processing, so that the PL intensity tend to decrease as processing time increasing, quenching the density of defects. Materials which exhibit a structural disorder at medium-range, show a large PL intensity than ordered ones [6, 63, 64 (a,b), 74 (a-c), 75 (a, b, c)]. Wherefore, it seems allowable to admit that the order-disorder relationship at medium range is associated with PL behavior, whose PL blue component is dominant, of the $NaNbO_3$ structures which tend to less disordered at medium-range with increasing of processing time.

According literature, PL emissions situated at high energy levels are related to the structural defects, such as strain and distortions lattice [84 a-e]. In this sense, the blue component can to be ascribed to the distortions on the NbO_6 octahedron owing to variations in the bond length (Nb-O) and bond angle variance (O-Nb-O), which undergo deviations along of processing time (see Tab. 2 and Tabs. S1, S2, S3 and S4). In general, the PL profiles observed arise from structural defects attributed to distortions of the NbO_6 octahedron, resulting in a structural disorder at medium-range, once blue component is dominant for all $NaNbO_3$ samples (>50 % see Fig. 8 and Tab. 4). The high PL intensity and broadening profile observed for $NaNbO_3$ processed in 30 minutes is a hard evidence which corroborates with decreasing E_{gap}, because it show a large defect density leading to a structural disorder at medium-range, responsible by the narrowing of the optical band gap. This structural disorder one manifest from defect density which are responsible by the broad band profile, so that blue PL component, comes from structural defects, is dominant under the another PL components (green and yellow), indicating that shallow levels were created within the band gap. Thus, the shallow levels density for $NaNbO_3$ (30 min) is larger because the deviations in the NbO_6 parameters (Tab. 2), between the $NaNbO_3$ synthesized, which give rise to the degree of disorder at medium-range are most pronounced.

Therefore, for $NaNbO_3$ structure whose the density of shallow levels is larger than density of deep levels, by the fact of the shallow levels are localized close to conduction band, contribute more effectively to PL intensity (Fig. 8 a), once the electrons photogenerated at conduction band can be most easily trapped by

CrystEngComm Accepted Manuscript

Please do notadjustmargins
View Article Online
DOI: 10.1039/C7CE00218A

Published on 25 May 2017. Downloaded by University of Lethbridge on 28/05/2017 21:08:29.

shallow levels and thus ones recombine with holes at valence band emitting the blue component. On other hands, the deep levels are localized regions more away to conduction band, so that the electrons photogenated can undergoes non-radiative decays until its positions, and from here ones recombine with holes at valence band emitting luminescence at low energy, *i.e.*, emitting the green and yellow PL components. The deep levels on the $NaNbO_3$ eletronic structure might to be associated to the surface defects, once luminescence at low energy comes from this kind defect [80, 84 a-e].

The degree of structural order-disorder in $NaNbO_3$ presents a symmetry breakage along the Nb–O bond lengths, resulting in complex clusters with different coordination numbers ($[NbO_6]-NbO_5$]) and/or in distortions of the $[NbO_6]-NbO_6]$ clusters [42 (a,b) 81 (a,b)]. The degree of the distortions and the extension of the bond lengths are responsible for generating electronic states within the band gap and/or for reorganizing them, promoting a local polarization effect, *i.e.*, and a charge gradient in the structure, thereby affecting the charge transfer process, for instance, in the case of photoluminescence [43, 75 (a,b,c), 81 (a,b), 84(c, d, e)].

The formation mechanism of the $[MO_6]$ and $[MO_5]$ clusters, more particularly the $[MO_5]$, (M = metal transition) involves a complex process of defects generation, where the changes in the M-O bond lengths, O-M-O bond angles can give rise to defects of oxygen vacancies localized both bulk and surface [85, 86, 87]. According to Kröger-Vink notation [86], to represent the point defect on the crystal, the oxygen vacancies are known to be the most common defects present in semiconductors and perovskite-oxide materials. These species can be present in three different charge states: neutral oxygen vacancy (V_O^x), singly occupied vacancy ($V_O^\bullet$) and empty oxygen vacancy ($V_O^{\bullet\bullet}$) states, which can capture up to two electrons, only one electron and no electron, respectively [80, 85, 86, 87]. The equations (1 and 2) below represent the formation process of the $NaNbO_3$ structure synthesized, in which from an ordered structure, under the presence of defects generated from changes in the Nb-O bond lengths and O-Nb-O bond angles, give rise to oxygen vacancies, undergo transformation into disordered structures.

$$[NbO_5.V_O^x] + [NbO_6]^x \rightarrow [NbO_5.V_O^\bullet] + [NbO_6]' \quad (1)$$

$$[NbO_5.V_O^\bullet] + [NbO_6]^x \rightarrow [NbO_5.V_O^{\bullet\bullet}] + [NbO_6]' \quad (2)$$

where $[NbO_6]^x$ is an electron acceptor; $[NbO_5.V_O^x]$ is an electron donor; and $[NbO_5.V_O^\bullet]$ can act both as electrons donor and acceptor. The $[NbO_6]^x$ clusters represent the most ordered structural forming unit of $NaNbO_3$ lattice.

According to the literature [63 a, 80, 88, 89], the electronic transitions between these species involve more than one kind of cluster. In other words, the cluster-to-cluster charge transfer (CCCT) plays an import role when it comes to both the formation and recombination process of photogenerated charges in the PL, which can be considered a novel class of electronic transitions involving the excitation/emission process.

Therefore, the PL behavior, at room temperature, observed here suggests that the most ordered structure of $NaNbO_3$ is comprised of only $[NbO_6]^x$ clusters on the lattice, which are transformed into $[NbO_5.V_O^x]$, $[NbO_5.V_O^\bullet]$ and $[NbO_5.V_O^{\bullet\bullet}]$ complex clusters. These clusters constitute the disordered fraction on the $NaNbO_3$ lattice due to the defects generated along of the processing by the microwave heating. The density of these defects generated depends of the extension in the Nb-O bond lengths and O-Nb-O bond angles, which consequently promote different degree distortions between neighbors clusters, and thereby a structural disorder at medium-range. However, as the processing time increases, there is a decline in these distortions, leading to less disordering to $NaNbO_3$ structure, decreasing the density of $[NbO_5.V_O^x]$, $[NbO_5.V_O^\bullet]$ and $[NbO_5.V_O^{\bullet\bullet}]$ complex clusters, and that of the intermediary energy levels within the band gap.

Lastly, the PL broad band exhibited by $NaNbO_3$ can be mainly attributed to presence of defects related to oxygen vacancies generated along processing time. The oxygen vacancies generated on the bulk are represented by the $[NbO_5.V_O^x]$ species, that comes from the large distortions between clusters ($[NbO_5.V_O^x]-[NbO_6]^x$), that consequently leads to a larger degree of disorder at medium-range, resulting in a considerable density of intermediary energy levels within the band gap close to conduction band (shallow levels), which are responsible by the blue PL component. On the other hands, the oxygen vacancies on the surface, arises of the lower distortion degree between clusters ($[NbO_5.V_O^\bullet]-[NbO_6]^x$ and $[NbO_5.V_O^{\bullet\bullet}]-[NbO_6]'$) that give rise to an density of deep levels responsible by the green and yellow PL component, which are represented by $[NbO_5.V_O^\bullet]$ and $[NbO_5.V_O^{\bullet\bullet}]$ complex clusters, respectively. The position occupied by the shallow and deep levels within the band gap obeys the energy associated to each intra-gap level associated to the oxygen vacanies ($V_O^x > V_O^\bullet > V_O^{\bullet\bullet}$) [85, 86, 87]. Thereby, the energy of the radiative decays related to each recombination process, occurs for the same energy order (blue > green > yellow).

Conclusions

In this work, we propose a hydrothermal method to obtain $NaNbO_3$ second phase-free via microwave heating in short synthesis time (30-90 minutes) and under minor processing temperature (180° C), than conventional methods reported in the literature. XRD pattern results obtained by Rietveld refinement and Raman scattering indicated a long- and short-range ordering of $NaNbO_3$, respectively, under crystallization with orthorhombic crystalline structure pertaining to the space group *Pbma*. Through FE-SEM images, we observed that self-assemble and Ostwald-ripening mechanisms can be responsible for the growth process of the particles in parallelepiped-like morphology as increasing processing time. UV-vis spectra showed that optical band gap undergoes slight increase as processing time also increases, due to density of structural defects generates along of processing time, which to leads to generation and/or reorganization of intermediary energy levels (shallows and deeps), thereby suggesting a possible structural disordering, once at long- and short-range the ordering is kept. The PL behavior at room temperature exhibited a broad band PL emission in the blue region (≈460 nm) which was decomposed in three components (blue-≈455nm, green≈530nm, and yellow≈610nm). The dominion of blue component implies that structural defects are presents into $NaNbO_3$ lattice, which lead to distortions between cluster However, these distortions and, consequently the disordering undergo decline as increasing processing time. The PL profile implies that these structural defects arise from the oxygen vacancies generated both bulk and surface, due to deviations in both the Nb-O bond lengths and in the O-Nb-O bond angles, and thereby leads to disorder at medium-range. These oxygen vacancies defects are able to transform $NaNbO_3$ ordered structure, represented by $[NbO_6]^x$ clusters, in $NaNbO_3$ structure with degree of order-disorder associated with the presence of

CrystEngComm Accepted Manuscript

Please do notadjustmargins

View Article Online
DOI: 10.1039/C7CE00218A

Published on 25 May 2017. Downloaded by University of Lethbridge on 28/05/2017 21:08:29.

$[NbO_5.V_O^x]$, $[NbO_5.V_O^{\bullet}]$ and $[NbO_5.V_O^{\bullet\bullet}]$ complex clusters. Depending on the extension of deviations in the bond lengths and bond angles, the distortion will be more or less able of to promote a electronic density, changing and/or reorganizing the intermediary energy levels within the band gap. Closer to conduction band the shallows levels, represented by the $[NbO_5.V_O^x]$ clusters, are responsible by the blue component, besides to be generated in larger density independently of processing time. The deep levels represented by the species $[NbO_5.V_O^{\bullet}]$ and $[NbO_5.V_O^{\bullet\bullet}]$ are responsible by green and yellow components, respectively, being presents in minor density into $NaNbO_3$ lattice.

Acknowledgments

The authors would like to express their deepest gratitude to Prof. Dr. Maximo Siu Li of São Carlos Physical Institute for providing the PL measurements, Prof. Dr. Juan Andreas of Universidad Jaume I Castelló de La Plana for theoretical discussion, and the Brazilian research agencies CAPES (Process: 88881.068060/2014-01), CNPq (Project: 402923/2014-6; Process: 157575/2015-2) and FAPESP-CEPID/CDMF 2013/07296-2 for granting financial support to the research group.

Notes and references

[1] K. V. Selvan and M. S. Mohamed Ali, *Renew. Sustain. Energy Rev.*, 2016, **54**, 1035-1047.
[2] J. Selvarathinam and A. Anpalagan, *IEEE Potentials*, 2016, **35**, 6-12
[3] M.-G. Kang, W.-S. Jung, C.-Y. Kang and S.-J. Yoon, *Actuators*, 2016, **5**, 5-22.
[4] I. Kanno, T. Ichida, K. Adachi, H. Koterab, Kenji Shibatac, T. Mishima, Sens Actuators A Phys., 2012, **179**, 132- 136
[5] J. Kim and J.-H. Koh, *J. Eur. Ceram. Soc.*, 2015, **35**, 3819-3825.
[6] (a) Y. Saito, H. Takao, T. Tani, T. Nonoyama, K. Takatori, T. Homma, T. Nagaya and M. Nakamura, Nature, 2004, **432**, 84. (b) J. Rödel, W. Jo, K. T. P. Seifert, E.-M. Anton, T. Granzow and D. Damjanovic, *J. Am. Ceram. Soc.*, 2009, **92**, 1153.
[7] D. Zhang, F. Shi, J. Cheng, X. Yang, E. Yan and M. Cao, *Ceram. Int.*, 2014, **40**, 14279-14285.
[8] M. A. L. Nobre, E. Longo, E. R. Leite, J.A. Varela, *Mater. Lett.* 1996, **28**, 215-220.
[9] B. Jaffe, W. R. Cook Jr, H. Jaffe. *Piezoelectric Ceramics*. London: Academic Press, 1971.
[10] (a) G. Li, Z. Yi, Y. Bai, W. Zhang, H. Zhang, H. *Dalton Trans.*, 2012, **41**, 10194-10198. (b) H. Shi, X. Li, D. Wang, Y. Yuan, Z. Zou, J. Ye, *Catal. Lett.*, 2009, **132**, 205. (c) K. Saito and A. Kudo, *Inorg. Chem.*, 2010, **49**, 2017. (d) G. Q. Li, N. Yang, W. L. Wang, W. F. Zhang, *J. Phys. Chem. C*, 2009, **113**, 14829. (e) K. Katsumata, S. Okazaki, C. E. J. Cordonier, T. Shichi, T. Sasaki, A. Fujishima, *ACS Appl. Mater. Interfaces*, 2010, **2**, 1236. (f) H. F. Shi, T. Z. Wang, J. Chen, C. Zhu, J. H. Ye, Z. G. Zou, *Catal. Lett.*, 2011, **141**, 525.
[11]. K. K. Mishra, V. Sivasubramanian and A. K. Arora, *J. Raman Spectrosc.*, 2011, **42**, 517.
[12] S. K. Mishra, N. Choudhury, S. L. Chaplot, P. S. R. Krishna and R. Mittal, *Phys. Rev. B: Condens. Matter Mater. Phys.*, 2007, **76**, 024110.
[13] H. D. Megaw, *Ferroelectrics*, 1974, **7**, 87.
[14] Y. Shiratori, A. Magrez, M. Kato, K. Kasezawa, C. Pithan and R. Wasert, *J. Phys. Chem. C*, 2008, **112**, 9610.
[15] Y. Shiratori, A. Magrez, J. Dornseiffer, F. H. Haegel, C. Pithan, and R. Waser, *J. Phys. Chem. B*, 2005, **109**, 20122.
[16] J. Koruza, J. Tellier, B. Malic, V. Bobnar, and M. Kosec, *J. Appl. Phys.*, 2010, **108**, 113509.
[17] S. K. Mishra, R. Mittal, V. Y. Pomjakushin, S. L. Chaplot, *Phys. Rev. B*, 2011, **83**, 134105.
[18] F. Tessier, R. Assabaa, R. Marchand, *J. Alloys Compd.*, 1997, **262-263**, 512.
[19] K. E. Johnston, C. C. Tang, J. E. Parker, K. S. Knight, P. Lightfoot and S. E. Ashbrook, *J. Am. Chem. Soc.*, 2010, **132**, 8732.
[20] S. K. Mishra, R. Mittal, V. Y. Pomjakushin and S. L. Chaplot, *Phys. Rev. B: Condens. Matter Mater. Phys.*, 2011, **83**, 134105.
[21] Z. X. Shen, X. B. Wang, M. H. Kuok and S. H. Tang, *J. Raman Spectrosc.*, 1998, **29**, 379.
[22]S. K. Mishra, M. K. Gupta, R. Mittal, S. L. Chaplot and T. Hansen, *Appl. Phys. Lett.*, 2012, **101**, 242907.
[23] K. E. Johnston, C. C. Tang, J. E. Parker, K. S. Knight, P. Lightfoot and S. E. Ashbrook, *J. Am. Chem. Soc*., 2010, **132**, 8732-8746
[24]-H. Maekawa, T. Nakao, S. Shimokawa and T. Yokokawa, *Phys. Chem. Miner*., 1997, **24**, 53.
[25] S. P. Solov'ev, Yu. N. Venevtsev, G. S. Zhdanov. and V. V. Ivanova, *Kristallografiya*, 1961, **78**, 171.
[26] C. N. W. Darlington and K. S. Knight, *Physica B*, 1999, **266**, 368.
[27] H. Xu, Y. Su, M. L. Balmer and A. Navrotsky, *Chem. Mater*., 2003, **15**, 1872.
[28] C. I. Cheon, H. W. Joo, K.-W. Chae, J. S. Kim, S. H. Lee, S. Torii and T. Kamiyama, *Mater. Lett.*, 2015, **156**, 214.
[29] W. J. Liu, *Electroceram*, 2013, **31**, 376.
[30] T. Rojac, M. Kosec, B. Mallic and J. Holc, *Sc. Sint., 2005, **37**, 61*
[31] A. Kikuchihara, F. Sakurai and T. Kimura, *J. Am. Ceram. Soc., 2012, **95**,* 1556-1562
[32] V. Samuel, A. B. Gaikwad and V. Ravi, Bull. Mater. Sci., 2006, **29**, 123.
[33] (a) Y. Lu, T. Karaki and T. Fujii, *Ceram. Int.*, 2015, **41**, S174. (b) A. J. Paula, M. A. Zaghete, E. Longo, J. A. Varela, *Eur. J. Inorg. Chem.*, 2008, **8**, 1300. (c) D. R. Modeshia, R. J. Darton, S. E. Ashbrook and R. I. Walton, *Chemm. Commun.*, 2009, **1**, 68.
[34] I. C. M. S. Santos, L. H. Lourerio, M. F. P. Silva, A. M. V. Cavaleiro, *Polyhedron*, 2002, **21**, 2009
[35] J. Wu and D. Xue, *Cryst. Eng. Comm.*, 2011, **13**, 3773. (b) H. Shi, X. Li, D. Wang, Y. Yuan, Z. Zou and J. Ye, *Catal. Letters*, 2009, **132**, 205.
[36] (a) C. O. Kappe, *Chimia*, 2006, **60**, 308. (b) B. Ondruschka ,W. Bonrath, *Chimia*, 2006, **60**, 326.
[37] (a) J. S. Schance, *Mol. Divers.*, 2003, **7**, 293. (b) D. E. Clark and W. H. Sutton, *Annu. Rev. Mater. Sci.*, 1996, **26**, 299.
[38] (a) J. P. Cheng, D. Agrawal, S. Komarneni, M. Mathis and R. Roy, *Mater. Res. Innov*, 1997, **1**, 44. (b) C. Gabriel, S. Gabriel, E. H. Grant, B. S. J. Halstead and D. M. P. Mingos, *Chem. Soc. Rev.*, 1998, **27**, 213.
[39] (a) S. W. Liu and J. P. Wightman, *J. Appl. Chem. Biotecnol*., 1971, **21**, 168. (b) R. N.Gedye, W.Rank and K. C. Westaway, *Can. J. Chem.*, 1991, **69**, 706. (c) R. Hicks and G. Majetich, *J. Microwave Power Electromagn. Eng., 1995,* **30**, 27.
[40] (a) M. D. Turner, R. L. Laurence, K. S. Yngvesson and W. C. Conner, *Catal. Lett.* 2001, **71**,133. (b) H. J. Kitchen, S. R. Vallance, J. L. Kenedy, N. Tapia-Ruiz, L. Carassiti, A. Harrison, A. G. Whittaker, T. D. Drysdale, S. W. Kingman and D. H. Gregory, *Chem. Rev.*, 2014, **114**, 1170.
[41] (a) K. Chatakondu, M. L. H. Green, D. M. P. Mingos, and *S.* M. Reynolds, *J. Chem. Soc., Chem. Commun.*1989, **20**, 1515. (b) W. C. Conner and G. A. Tompsset, *J. Phys. Chem. B*, 2007, **112**, 2110.
[42] A. Abu-Sharma, J. S. Morris and S. R. Koirtyohann, *Anal. Chem.*, 1975, **47**, 1475.

CrystEngComm Accepted Manuscript

Please do notadjustmargins
View Article Online
DOI: 10.1039/C7CE00218A

Published on 25 May 2017. Downloaded by University of Lethbridge on 28/05/2017 21:08:29.

[43] G. F. Teixeira, T. R. Wright, D. C. Manfroi, E. Longo, J. A. Varela, M. A. Zaghete. Mater. Lett., 2015, **139**, 443.
[44] J. H. Jung, C.-Y. Chen, W.-W. Wu, J.-I. Hong, B. K. Yun, Y. Zhou, N. Lee, W. Jo, L.-J. Chen, L.-J. Chou and Z. L. Wang, *J. Phys. Chem. C*, 2012, **116**, 22261.
[45] M. Sakata, M. J. Cooper, *J. Appl. Cryst.*, 1979, **12**, 554.
[46] (a) H. M. Rietveld, *Acta Cryst.*, 1967, **2**, 65. (b) H. M. Rietveld, *J. Appl. Cryst.*,1969, **2**, 65.
[47] G. S. Pawley, *J. Appl. Cryst.*, 1981, **14**, 357.
[48] G. Will, Powder diffraction: The Rietveld method and the two stage method to determine and refine crystal structures from powder diffraction data, Springer-Verlag Berlin Heidelberg, 2006, pp. 44–69.
[49] L. Lutterotti, M. Bortolotti, G. Ischia, I. Lonardelli and H. R. Wenk, *Z. Kristallogr. Suppl.*, 2007, **26**, 125.
[50] A. C. Larson, R. B. Von Dreele, GSAS: general structure analysis system (GSAS). [Los Alamos: Los Alamos National Laboratory], 2001. Software.
[51] B. H. Toby, *J. Appl. Cryst.*, 2001, **34**, 210.
[52] X. Hongwu, S. Yali, B. M. Lou and N. Alexandra. *Chem. Mater.*, 2003, **15**, 1872.
[53] H. Zhu, Z. Zheng, X. Gao, Y. Huang, Z. Yan, J. Zou, H. Yin, Q. Zou, S. H. Kable, J. Zhao, Y. Xi, W. N. Martens and R. L. Frost, *J. Am. Chem. Soc.*, 2006, **8**, 2373.
[54] S. Y. Wu, X. Q. Liu and X. M. Chen, *Ceram. Int.*, 2010, **36**, 871.
[55] S. Komarneni, Y. D. Noh, J. Y. Kim, S. H. Kim and H. Katsuki, *ChemInform*, 2010, **41**, 1033.
[56] P. Li, S. X. Ouyang, G. C. Xi, T. Kako and J. H. Ye, *J. Phys. Chem. C*, 2012, **116**, 7621.
[57]. J. L. Garcia-Munoz, J. Rodriguezcarvajal, P. Lacorre, and J. B. Torrance,. *Phys. Rev. B.*, 1992, **46**, 4414.
[58] V. M. Goldschmidt, T. Barth, G. Lunde and W. Zachariasen. *Geochemische Verteilungsgesetze der Elemente – VII. Die Gesetze der Krystallochemie*, NSkr. Nor. Vidensk.–Akad., [KI.] I: Mat.–Naturvidensk. KI;Oslo 2, 1-117 (1926).
[59] R. D. Shannon, *Acta Crystallogr., Sect. A: Cryst. Phys., Diffr. Theor. Gen. Crystallogr.*, 1976, **A32**, 751.
[60] R. I. Hines, PhD thesis, University of Bristol, 1997
[61] A. Navrotsky, *Physics and Chemistry of Earth Materials*, ed. A. Navrotsky, Cambridge University Press, 1994, Chapter 5, pp. 172–272.
[62] S. K. Sahu, S. Zlotnik, A. Navrotskya and P. M. Vilarinho, *J. Mater. Chem. C*, 2015, **3**, 7691
[63] (a). L. S. Cavalcante, V. M. Longo, J. C. Sczancoski, M. A. P. Almeida, A. A. Batista, J. A. Varela, M. O. Orlandi, E. Longo and M. Siu Li, *CrystEngComm*, 2012, **14**, 853. (b) L. S. Cavalcante, M. A. P. Almeida, W. Avansi, Jr., R. L. Tranquilin, E. Longo, N. C. Batista, V. R. Mastelaro, and M. Siu Li, *Inorg. Chem.*, 2012, **51**, 10675. (c) L. S. Cavalcante, J. C. Sczancoski, L. F. Lima, Jr., J. W. M. Espinosa, P. S. Pizani, J. A. Varela and E. Longo, *Cryst. Growth Des.*, 2009, **9**, 1002. (d) J. C. Sczancoski, L. S. Cavalcante, M. R. Joya, J. W. M. Espinosa, P. S. Pizani, J. A. Varela and E. Longo, *J. Colloid Interface Sci.*, 2009, **330**, 227
[64] (a) V. S. Marques, L. S. Cavalcante, J. C. Sczancoski, A. F. P. Alcântara, M. O. Orlandi, E. Moraes, E. Longo, M. S. Li and M. R. M. C. Santos, *Cryst. Growth Des.*, 2010, **10**, 4752. (b) X.-Z. Wang, *J. Mater. Sci.: Mater. Electron.*, 2014, **25**, 3271
[65]. K. Momma and F. Izumi, *J. Appl. Crystallogr.*, 2011, **44**, 1272.
[66] Y. D. Juang, S. B. Dai, Y. C. Wang, J. S. Hwang, M. L. Hu and W. S. Tse. J. *Appl. Phys*., 2000, **88**, 742.
[67] S. E. Ashbrook, L. Le Pollès, R. Gautier, C.J. Pickardzc and R. I. Walton., *Phys. Chem. Chem. Phys.*, 2006, **8**, 3423.
[68] (a) A. M. George and J. F. Stebbins, *Am. Mineral.*, 1995, **80**, 878. (b) H. Maekawa, T. Nakao, S. Shimokawa and T. Yokokawa, *Phys. Chem. Miner.*, 1997, **24**, 53. (c) V. A. Shuvaeva, M. Y. Antipin, S. V. Lindeman, O. E. Fesenko, V. G. Smotrakov and Y. T. Struckov, *Kristallografiya*, 1992, **37**, 1502. (d) J. F. Stebbins, I. Farnan, N. Dando and S. Y. Tzeng, *J. Am. Ceram. Soc.*, 1992, **75**, 3001.
[69] S. D. Ross, *J. Phys. C*., 1970, **3,** 1785.
[70] F. D. Hardcastle and I. E. Wachs, *Solid State Ionics*, 1991, **45**, 201.
[71] Y. D. Juang, S. B. Dai, Y. C. Wang, W. Y. Chou, J. S. Hwang, M. L. Hu and W. S. Tse, *Solid State Commun.*, 1999, **111**, 723.
[72] T. Zhang, K. Zhao, J. Yu, J. Jin, Y. Qi, H. Li, X. Hou and G. Liu, *Nanoscale*, 2013, **5**, 8375.
[73] Y. Chang, Z.Yang, M. Dong, Z. Liu, Z. Wang. *Mater.Res. Bull*. , 2009, **44**, 538.
[74] (a) G. J. Wilson, A. S. Matijasevich, D. R. G. Mitchell, J. C. Schulz and G. D. Will, *Langmuir*, 2016, **22**, 2016. (b)M. Lin, Z. Y. Fu, H. R. Tan, J. P. Y. Tan, S. C. Ng and E. Teo, *Cryst. Growth Des.*, 2012, **12**, 3296. (c) A. P. de Moura, L. H. de Oliveira, P. F. S. Pereira, I. L. V. Rosa, M. S. Li, E. Longo and J. A. Varela, *Adv. Chem. Eng. Sci.*, 2012, **2**, 465.
[75] (a)E. Orhan, M. Anicete-Santos, M. A. M. A. Maurera, F. M. Pontes, A. G. Souza, J. Andres, A. Beltran, J. A. Varela, P. S. Pizani, C. A. Taftf and E. Longo, *J. Solid State Chem.*, 2005, **178**, 1284 (b) E. Silva Junior, F. A. La Porta, M. S. Liu, J. Andrés, J. A. Varela and E. Longo. Dalton Trans., 2015, **44**, 3159. (c) E. Orhan, M. Anicete-Santos, M. A. Maurera, F. M. Pontes, C. O. Paiva-Santos, A. G. Souza, J. A. Varela, P. S. Pizani, E. Longo, *Chem. Phys*., 2005, **312** ,1.
[76] P. W. Voorhees, *J. Stat. Phys.*, 1985, **38**, 231.
[77] P. Li, H. Xu, L. Liu, T. Kako, N. Umezawa, H. Abe and J. Ye, *J. Mater. Chem. A*, 2014, **2**, 5606.
[78] J. H. Nobbs, *Rev. Prog. Coloration, 1985, **15**, 66-75*
[79] B. Zielińska, E. Borowiak-Palen and R. J. Kalenczuk, *J. Phys. Chem. Solids*, 2011, **72**, 117.
[80] E. A. V. Ferri, J. C. Sczancoski , L. S. Cavalcante, E. C. Paris , J. W. M. Espinosa, A. T. de Figueiredo, P. S. Pizani, V. R. Mastelaro, J. A. Varela b, E. Longo, *Mater. Chem. Phys.*, 2009, **117**, 192.
[81] (a) J. Marzin, J. Gérard, A. Izraël, D. Barrier and G. Bastard, *Phys. Rev. Lett.*, 1994, **73**, 716; (b) N. Greenham, X. Peng and A. Alivisatos, *Phys. Rev. B: Condens. Matter*, 1996, **54**, 17628.
[82] (a) E. Almeida, L. de S. Menezes, C. B. de Araújo, A. A. Lipovskii, *J. Appl. Phys.*, 2011,**109**,113108. (b) V. S. Marques, L. S. Cavalcante, J. C. Sczancoski, D. P. Volanti, J. W. M. Espinosa, M. R. M. Joya, *Solid State Sci.*, 2008,**10**, 1056.
[83] JANDEL SCIENTIFIC. Peakfit. Version 4.0. San Rafael, 1995
[84] (a) A. K. Ghosh, F. G. Wakim and R. R. Jr. Addiss,. *Phys. Rev*., 1969, **184**, 979. (b) J. Liu, J. Li, A. Sedhain, J. Lin and H. Jiang, *J. Phys. Chem. C*, 2008, **112**, 17127. (c) V. M. Longo, A. T. de Figueiredo, S. de Lazaro, M. F. Gurgel, M. G. S. Costa, C. O. Paiva-Santos, J. A. Varela, E. Longo, V. R. Mastelaro, F. S. de Vicente, A. C. Hernandes, R. W. A. Franco, *J. Appl. Phys.*,2008, **104**, 023515. (d) V. M. Longo, L. S. Cavalcante, A. T. de Figueiredo, L. P. S. Santos, E. Longo, J. A. Varela, J. R. Sambrano, C. A. Paskocimas, F. S. De Vicente and A. C. Hernandes, *Appl. Phyis. Lett.*. 2007, **90**, 91906. (e) X. Yang, I. D. Williams, J. Chen, J. Wang, H. Xu, H. Konishi, Y. Pan, C. Liang and M. Wu, *J. Mater. Chem*., 2008, **18**, 3543.
[85] T. Yamamoto and T. Ohno, *Phys. Chem. Chem. Phys., 2012, **14**, 589-598.*
[86] Q. Zhu, C. Xie, H. Li, C. Yang, S. Zhang and D. Zeng. *J. Mater. Chem. C, 2014, **2**, 4566.*
[87] D. Li, Y. H. Leung, A. B. Djurišić, Z. T. Liu and M. H. Xie, *Appl. Phys. Lett. 2004, **85**, 1601-1603.*
[88] F. R. Kröger, H. J. Vink, *Solid State Phys.*, 1956, **3**, 307.

CrystEngComm Accepted Manuscript

Please do notadjustmargins

View Article Online
DOI: 10.1039/C7CE00218A

[89] V. M. Longo, L. S. Cavalcante, E. C. Paris, J. C. Sczancoski, P. S. Pizani, M. S. Li, J. A. Andrés, E. Longo and J. A. Varela, *J. Phys. Chem. C*, 2011, **115**, 5207.

Published on 25 May 2017. Downloaded by University of Lethbridge on 28/05/2017 21:08:29.

CrystEngComm Accepted Manuscript

View Article Online
DOI: 10.1039/C7CE00218A

Published on 25 May 2017. Downloaded by University of Lethbridge on 28/05/2017 21:08:29.

CrystEngComm Accepted Manuscript

Table Caption

Table 1: $NaNbO_3$ lattice parameters and reliability factors from Rietveld refinement method.

Table 2: Bond lengths (Nb-O), bond angles (O-Nb-O), polyhedral volume, and coordination number of NbO_6 octahedron of the $NaNbO_3$ obtained by MAH method and the theoretical values reported in the literature (CIG ICSD n°. 96779).

Table 3: Raman peaks position observed in Raman spectra of $NaNbO_3$ obtained by MAH method at different processing time compared with literature.

Table 4: PL intensity, FWHM and peaks centers of the broad band profiles and PL components of $NaNbO_3$ obtained by MAH method at different processing time compared with literature.

View Article Online
DOI: 10.1039/C7CE00218A

Published on 25 May 2017. Downloaded by University of Lethbridge on 28/05/2017 21:08:29.

Table 1

$NaNbO_3$ – CIF 96779 [45]				
Atoms	**Wyckoff**	**x**	**y**	**z**
Na1	4c	0.75000	0	0.23400
Na2	4d	0.74300	0.25000	0.24000
Nb1	8e	0.25830	0.12600	0.24620
O1	4c	0.25000	0	0.31100
O2	4d	0.24020	0.25000	0.18170
O3	8e	0.06790	0.13970	0.54430
O4	8e	0.49190	0.11020	-0.01190
volume = 476.91 Å^3; *a* = 5.5625 Å; *b*= 15.5495 Å ; *c* = 5.5138 Å. and Space group: *Pbma*				
$NaNbO_3$ – 30 minutes				
Atoms	**Wyckoff**	**x**	**y**	**z**
Na1	4c	0.75000	0	0.23720
Na2	4d	0.78726	0.25000	0.23278
Nb1	8e	0.26363	0.12465	0.25339
O1	4c	0.25000	0	0.32959
O2	4d	0.25548	0.25000	0.20790
O3	8e	0.05073	0.14267	0.52816
O4	8e	0.48029	0.11132	-0.02110
R_{wp} = 6.05 %; R_{exp} = 5.41 %; R_B = 2,98 %; χ^2 = 1.25; volume = 477.6242 Å^3; *a* = 5.56603 Å, *b* = 15.56152 Å, *c* = 5.51428 Å and Space group: *Pbma*				
$NaNbO_3$ – 60 minutes				
Atoms	**Wyckoof**	**x**	**y**	**z**
Na1	4c	0.75000	0	0.25894
Na2	4d	0.78875	0.25000	0.26569
Nb1	8e	0.26560	0.12478	0.24921
O1	4c	0.25000	0	0.28548
O2	4d	0.25616	0.25000	0.17236
O3	8e	0.05256	0.14603	0.53277
O4	8e	0.48209	0.11318	-0.02714
R_{wp} = 5.97 %; R_{exp} = 5.47 %; R_B = 2,81%; χ^2 = 1.19; volume = 477.6392 Å^3; *a* = 5.56709 Å, *b* = 15.56150 Å, *c* = 5.51341 Å and Space group: *Pbma*				
$NaNbO_3$ – 90 minutes				
Atoms	**Wyckoof**	**x**	**y**	**z**
Na1	4c	0.75000	0	0.26320
Na2	4d	0.78321	0.25000	0.26474
Nb1	8e	0.26442	0.12477	0.24731
O1	4c	0.25000	0	0.30125
O2	4d	0.25409	0.25000	0.18275
O3	8e	0.06456	0.14254	0.52942
O4	8e	0.49013	0.11089	-0.02136
R_{wp} = 5.84 %; R_{exp} = 5.08 %; R_B = 3,24%; χ^2 = 1.16; volume = 477.5946 Å^3; *a* = 5.56798 Å, *b* = 15.55615 Å, *c* = 5.51391 Å and Space group: *Pbma*				

CrystEngComm Accepted Manuscript

View Article Online
DOI: 10.1039/C7CE00218A

Published on 25 May 2017. Downloaded by University of Lethbridge on 28/05/2017 21:08:29.

Table 2

NbO_6 octahedron parameters	$NaNbO_3$ CIF ICSD n°. 9766	$NaNbO_3$ 30 min	$NaNbO_3$ 60 min	$NaNbO_3$ 90 min
Average bond length (Nb-O) (Å)	1.9885	1.9844	1.9870	1.9851
Polyhedral volume (Å^3)	10.4112	10.3910	10.4127	10.3979
Distortion index	0.01672	0.01610	0.01157	0.01832
Bond angle variance (deg^3)	15.4624	5.4291	10.5047	5.8160
Effective coordination number	5.8886	5.9246	5.9591	5.8562

CrystEngComm Accepted Manuscript

View Article Online
DOI: 10.1039/C7CE00218A

Published on 25 May 2017. Downloaded by University of Lethbridge on 28/05/2017 21:08:29.

Table 3

Raman vibrational modes	This work	Ref [24]	Ref [71]
v_1	600 cm^{-1}	599.4-613.3 cm^{-1}	605
v_2	560 cm^{-1}	556.4-569.4 cm^{-1}	560 cm^{-1}
v_3	-	670.6 cm^{-1}	-
v_4	429 cm^{-1}	377.3, 433.1 cm^{-1}	375, 433 cm^{-1}
v_5	206-276 cm^{-1}	~200-300 cm^{-1}	223, 258, 279 cm^{-1}
v_6	180 cm^{-1}	170 cm^{-1}	180-186 cm^{-1}
v_1+ v_5	870 cm^{-1}	870.6 cm^{-1}	-

CrystEngComm Accepted Manuscript

View Article Online
DOI: 10.1039/C7CE00218A

Published on 25 May 2017. Downloaded by University of Lethbridge on 28/05/2017 21:08:29.

Table 4

Proc. time	**30 min**			**60 min**			**90 min**		
FWHM Broad band **(nm)**	138.20			145.84			203.41		
PL components	blue	green	yellow	blue	green	yellow	blue	green	yellow
Area (%)	57	30	13	55	28	17	50	30	20
FWHM PL comp. **(nm)**	80.58	80.31	80.58	84.48	85.35	85.78	109.17	105.95	100.48
PL components peak center (nm)	455	530	610	455	530	610	455	530	610

CrystEngComm Accepted Manuscript

View Article Online
DOI: 10.1039/C7CE00218A

Published on 25 May 2017. Downloaded by University of Lethbridge on 28/05/2017 21:08:29.

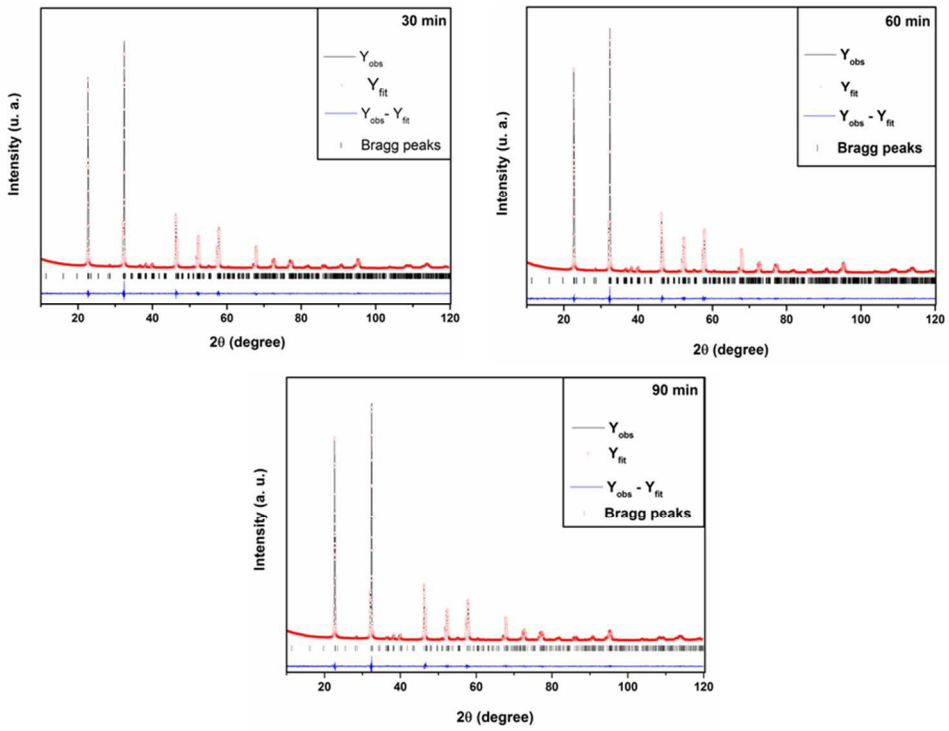

XRD patterns from Rietveld refinement of $NaNbO_3$ heat treated at 180 °C from MAH method under different processing times.

254x190mm (96 x 96 DPI)

CrystEngComm Accepted Manuscript

View Article Online
DOI: 10.1039/C7CE00218A

Published on 25 May 2017. Downloaded by University of Lethbridge on 28/05/2017 21:08:29.

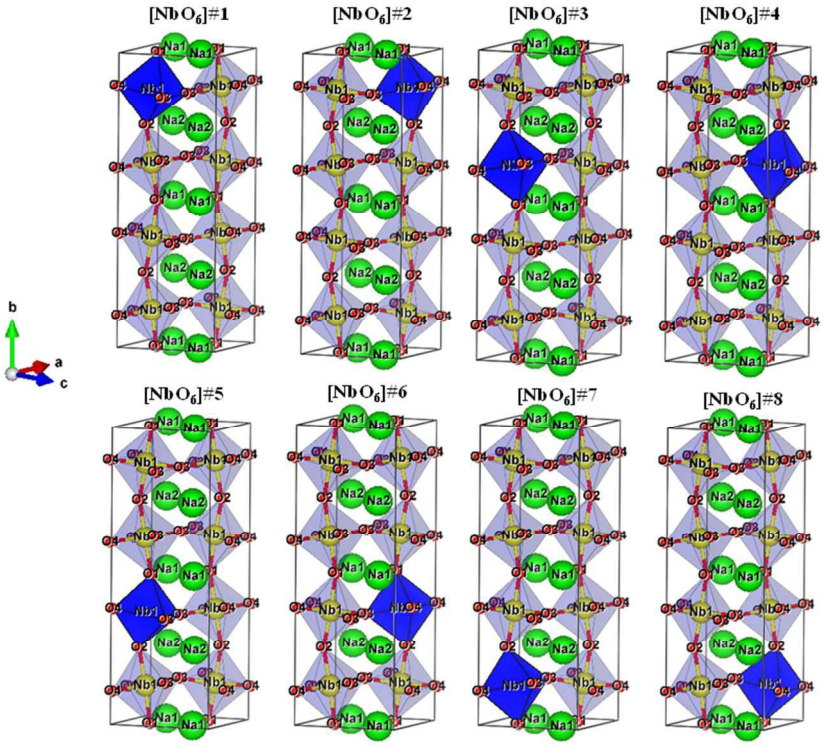

Unit cell representations of $NaNbO_3$ obtained by MAH method

254x190mm (96 x 96 DPI)

CrystEngComm Accepted Manuscript

View Article Online
DOI: 10.1039/C7CE00218A

Published on 25 May 2017. Downloaded by University of Lethbridge on 28/05/2017 21:08:29.

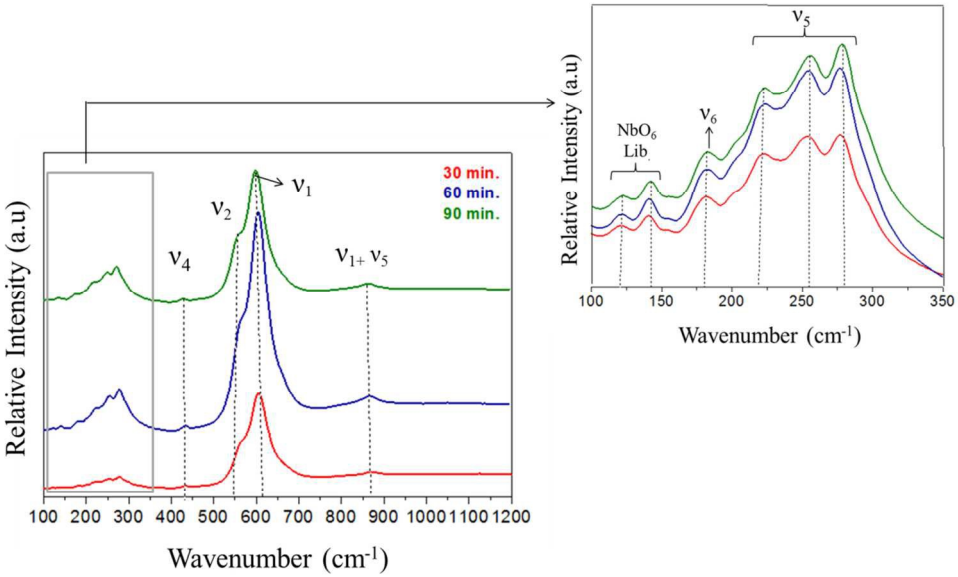

Raman spectra of $NaNbO_3$ obtained by MAH method for different processing time (30, 60 and 90 minutes).

343x205mm (96 x 96 DPI)

CrystEngComm Accepted Manuscript

View Article Online
DOI: 10.1039/C7CE00218A

Published on 25 May 2017. Downloaded by University of Lethbridge on 28/05/2017 21:08:29.

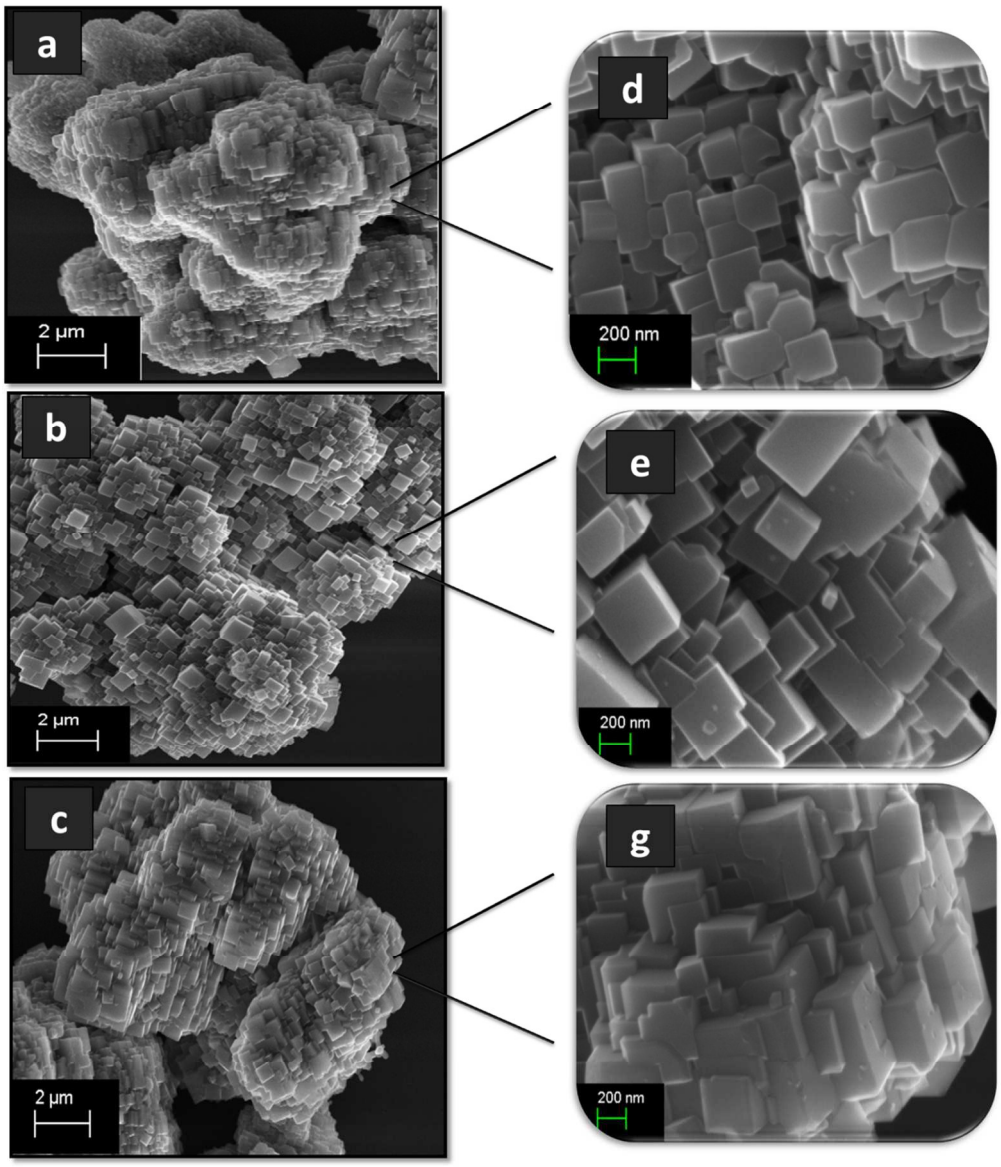

FE-SEM images of NaNbO3 particles obtained by MAH method for distinct processing time: (a-d) 30 min. (b-e) 60 min and (c-f) 90 min.

344x400mm (96 x 96 DPI)

CrystEngComm Accepted Manuscript

View Article Online
DOI: 10.1039/C7CE00218A

Published on 25 May 2017. Downloaded by University of Lethbridge on 28/05/2017 21:08:29.

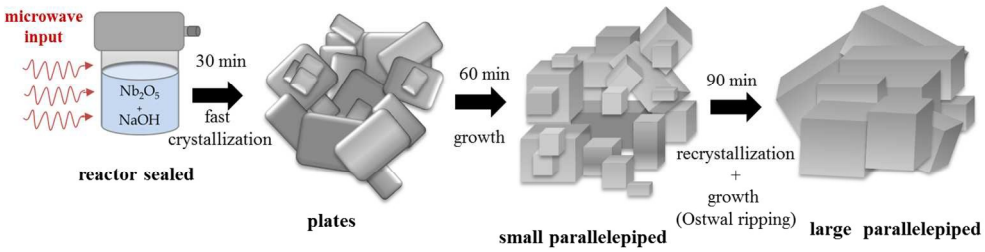

Growth mechanism of $NaNbO_3$ particles obtained by MAH.

392x103mm (96 x 96 DPI)

CrystEngComm Accepted Manuscript

View Article Online
DOI: 10.1039/C7CE00218A

Published on 25 May 2017. Downloaded by University of Lethbridge on 28/05/2017 21:08:29.

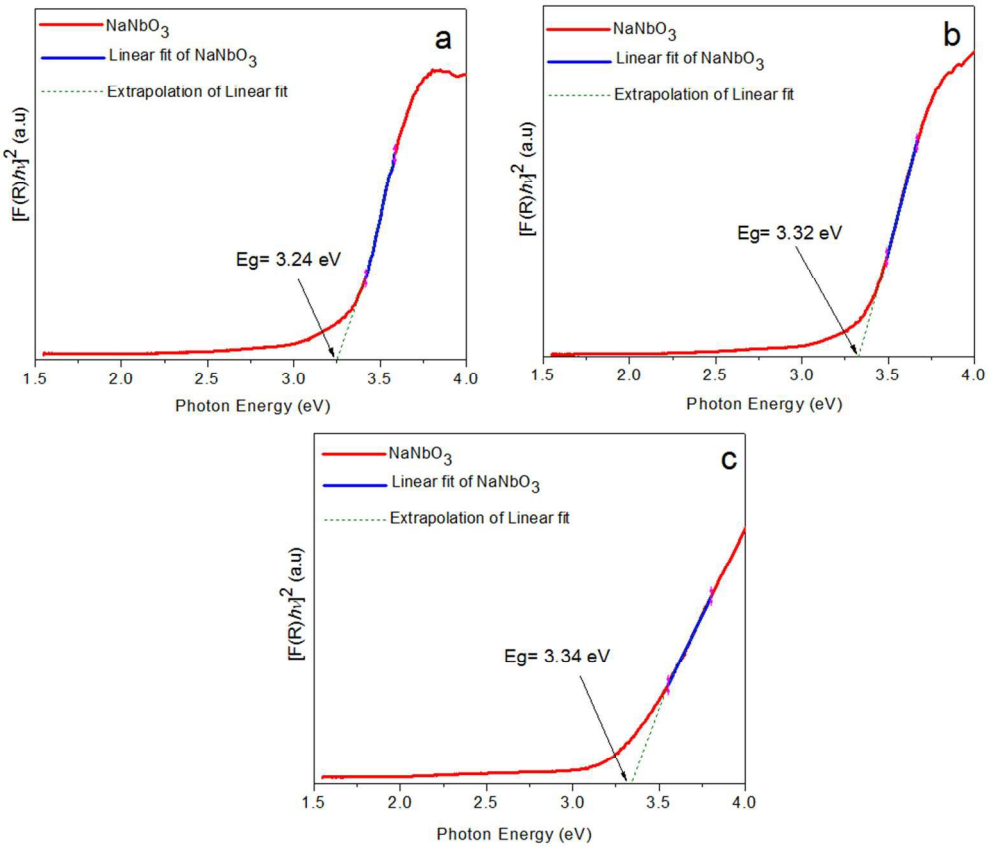

UV-visible spectra of $NaNbO_3$ obtained by microwave hydrothermal method for different processing time: (a) 30 min. (b) 60 min and (c) 90 min.

271x234mm (96 x 96 DPI)

CrystEngComm Accepted Manuscript

View Article Online
DOI: 10.1039/C7CE00218A

Published on 25 May 2017. Downloaded by University of Lethbridge on 28/05/2017 21:08:29.

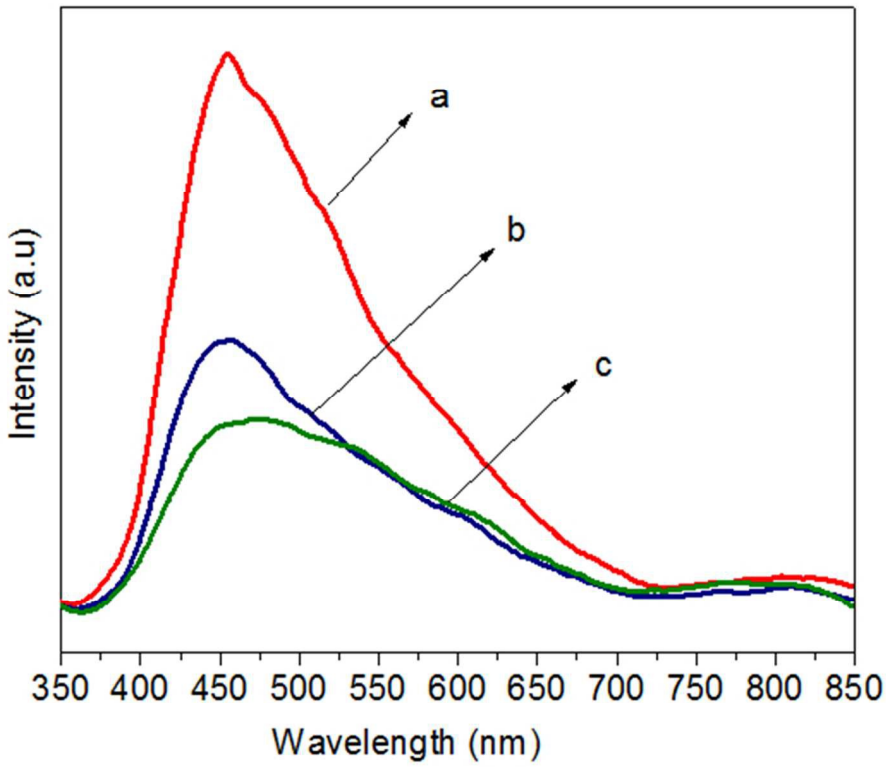

Photoluminescence spectra of $NaNbO_3$ powders obtained by MAH method for different processing time: (a) 30 min. (b) 60 min and (c) 90 min.

154x125mm (96 x 96 DPI)

CrystEngComm Accepted Manuscript

View Article Online
DOI: 10.1039/C7CE00218A

Published on 25 May 2017. Downloaded by University of Lethbridge on 28/05/2017 21:08:29.

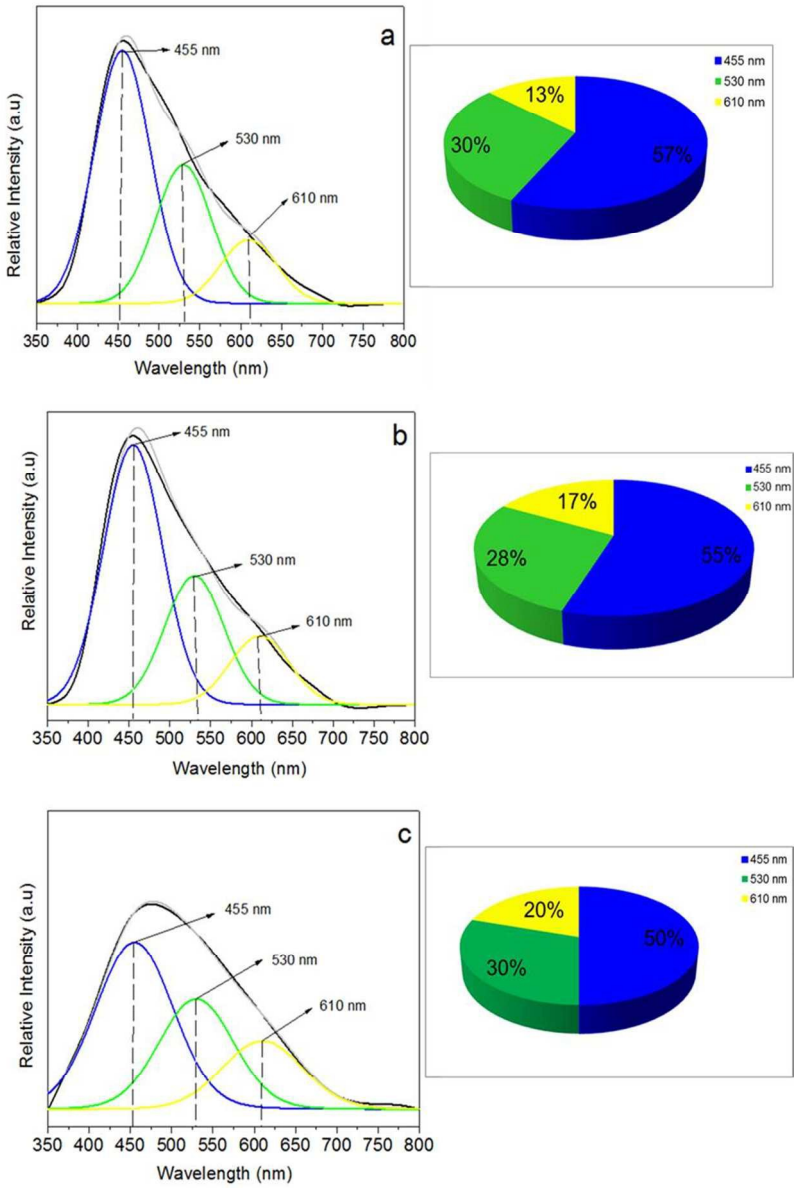

Deconvolution of PL spectra of $NaNbO_3$ powders obtained by microwave hydrothermal method for different processing time: (a) 30 min. (b) 60 min and (c) 90 min.

164x244mm (150 x 150 DPI)

CrystEngComm Accepted Manuscript

View Article Online
DOI: 10.1039/C7CE00218A

Published on 25 May 2017. Downloaded by University of Lethbridge on 28/05/2017 21:08:29.

Highlights

Unveiling the correlation between structural order-disorder character and photoluminescence emissions of $NaNbO_3$

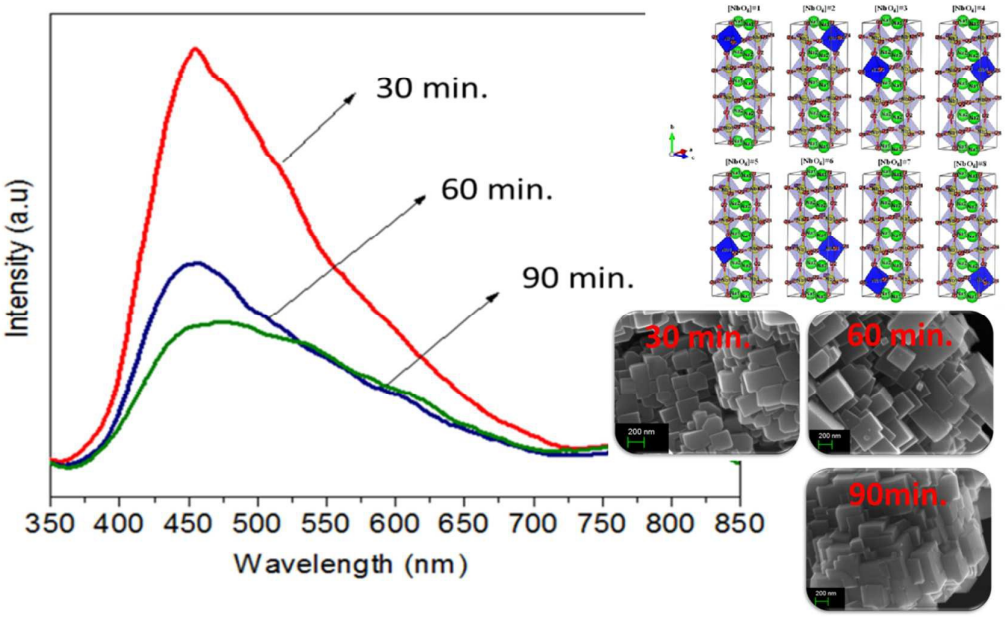

Orthorhombic $NaNbO_3$ particles obtained by MAH route show photoluminescence emission is related to structural disorder effect at medium range.

CrystEngComm Accepted Manuscript